Journal of Materials and Electronic Devices 6 (2021) 7-15

JOURNAL OF
MATERIALS AND ELECTRONIC DEVICES
JMED
http://dergi-fytronix.com/

Transition metals (Cu/Co/Mn) doped NiO films: Structural, optical and morphological properties

Olcay GENÇYILMAZ

Çankırı Karatekin University, Çerkeş Vocational School, Department of Material and Material Processing Technologies, 18100-Çankırı, Turkey

This paper reports a work of the produce of un-doped and transition metals doped nickel oxide (NiO) films and its some physical properties characterization. The un-doped, Cu, Co and Mn doped NiO films were produced by spray pyrolysis technique and investigated the dopant elements effects of on structural, morphological and optical properties. X-ray diffraction results revealed that the sprayed NiO films were polycrystalline structures in cubic phase and exhibit (111) preferential orientation. Moreover, the crystalline levels and peak positions were slightly changed by doping. The average grain size of the films was calculated using Scherer formula and Williamson and Hall plots. Also, the optical parameters such as band gap energy, Urbach energy, steepness parameter, refractive index and dielectric constants were calculated using absorption spectra and energy gap-refractive index relations (Moss Relation and Herve- Vandamme). The band gap values of NiO films were determined in range of 3.55-3.20 eV. From the FESEM investigations, the surface morphology of the NiO films was found to depend on the doped element. The chancing of the physical properties and its correlation to doped transition metals were discussed by means of the results procured in the work.

Keywords: NiO films; Transition metals doping; Optical constants; XRD; FESEM

Submission date: 20 May 2021

Acceptance Date: 22 October 2021

**Corresponding author. Tel: +90 376 218 9500; Fax: -*
E-mail address: ogencyilmaz@karatekin.edu.tr (Olcay Gençyılmaz)

1. Introduction

In recent years, nickel oxide (NiO) films are extensively researched and developed because of high availability in various technological applications. NiO is very important p-type and semitransparent semiconductor with stable and wide bad gap (3.6-4.0 eV) [1, 2]. NiO films has been widely potential application areas such as gas sensors, electrochromic devices, magnetic materials, catalysis, solar thermal absorber fuel cell electrodes due to its suitable and improvable optical, electrical and structural properties [3-11]. NiO films can be produced by various techniques, both chemical and physical such as sol-gel method, reactive sputtering, chemical deposition, thermal evaporation, chemical vapor deposition, electrochemically deposition, spray pyrolysis [12-21]. Among them, the spray pyrolysis technique has many advantages: (i) it includes high deposition rates, (ii) it is a low-cost and simple technique, (iii) it allows the possibility of obtaining films with a large area, (iv) it does not require to vacuum, (v) it is reproducible, (vi) it is non-planer geometries, (vii) control of stoichiometry. Doping is a fundamental technique to control the properties of semiconductors and to obtain new multifunctional technological materials. In order to provide some interesting properties, nickel oxide was doped by several elements such as lithium, aluminum, chrome, iron, cobalt, tungsten, manganese [22-24]. Now it is well known that the physical properties of NiO films can be controlled by doping with metallic ions due to physical and chemical properties of NiO films strongly depend on their size and shape. But doping NiO films prepared by spray pyrolysis technique with transition metals such as Mn, Fe, Co and Cu is very rare in literature.

For these reason, in this work, we have focused the effects of transition metals as doped on structural, optical and morphological properties of un-doped and Cu- Co-Mn doped NiO films by spray pyrolysis.

2. Material and Methods

Un-doped and doped NiO films were deposited on a glass substrate by spray pyrolysis technique. Before the start of the deposition process, the glass substrates were cleaned thoroughly using warm acetone and methanol. Finally, substrates were ultrasonically cleaned with deionized water. Table 1 shows the experimental parameters for NiO films synthesis in detail. The precursor spraying Nickel nitrate hexahydrate solutions was sprayed onto the glass substrates through a glass nozzle. When aerosol droplets come close to the substrates, highly adherent films were produced due to the pyrolytic process resulting in the formation of NiO films according to the following reaction:

$$Ni(NO_3)2.6H_2O \rightarrow NiO + 2NO_2 + 1/2O_2 + 6H_2O \quad (1)$$

The un-doped NiO film was obtained as brownish and transparent while the other doped films were found to be blackish hue. The thickness of un-doped and doped NiO films was measured by weighing method using digital weight balance (Ohaus-Pioneer). The thickness was calculated using formula;

$$T=\Delta W/\rho A \quad (2)$$

where T is film thickness, ΔW is the difference in weight of substrate before and after film deposition, A is the area of the film in cm^2, ρ is the density of the film (ρ= 6.67 gr/cm^3). The thickness of the NiO films was estimated in the range of 483–495 nm. change in doped NiO film is attributed to the existence of doped element.

Table 1. Experimental parameters

Synthesis films	NiO and Cu/Co/Mn doped NiO
Solution source	Nickel nitrate hexahydrate [$Ni(NO_3)_2.6H_2O$] Copper Nitrate [$Cu(NO_3)_2$] Cobalt nitrate [$Co(NO_3)_2$] Manganese nitrate [$Mn(NO_3)_2$] Deionized water
Doped and Flow rate	3 % - 5 cc/dk
Amount and Molarity of solution	100 ml - 0.01 M
Spraying time-Substrate temperature	20 dk - 450±5°C
Distance between substrate and atomizer-Carrier gas-Pressure	~25 cm-Nitrogen - 0.2 Bar

The structural, surface and optical properties of NiO films were examined using various characterization techniques. Characterizations of the all films were performed at room temperature. Table 2 shows list of parameters determined and equipment used for this purpose. To examine the structure of the films, a Bruker X-ray Diffractometer (D8 Advance XRD) with Cu Kα line (λ=1.5406 Å), was used. The optical measurements of films were evaluated using Shimadzu UV - 2550 UV- VIS spectrophotometer at wavelength range of λ=300-900 nm. The band gap energy values for these films were calculated by optic method. Also, Urbach energy, refractive index and dielectric constants were determined using UV spectrophotometer data. The surface morphological study was carried out using a field emission scanning electron microscopy (FESEM Zeiss Ultra Plus).

Table 2. List of parameters determined and equipment used for this purpose.

Characterization Equipments	**Determined Parameters**
Bruker D8 Advance XRD diffractometer	Structural analysis Crystal structure Lattice parameter Texture coefficients Lattice strain Crystallite size
Shimadzu UV -2550 UV- VIS spectrophotometer	Absorbance spectra Band gap energy Urbach energy Refractive index Dielectric constants Steepness parameter
A field emission scanning electron microscopy (FESEM Zeiss Ultra Plus)	Surface morphology

4. Results and discussion

4.1. Structural characterization

Fig. 1 shows the XRD patterns of un-doped and doped NiO films. XRD patterns show that all films were grown onto the glass substrates present good crystallinity. All the patterns exhibit a face centered cubic crystal structure with diffraction peaks at (111), (200), (220), and (311). The peaks were indexed by comparing our XRD data with the Bunsenite JCSPD card No: 47-1049 for NiO. All patterns exhibit a cubic structure without any additional impurity phase, indicating that the structure is not affected by Cu/Mn/Co substitution. For all dopant elements, no evidence of secondary phases or phases other than that of NiO is found which indicates that the Cu/Mn/Co dopant elements get substituted at the Ni site without affecting the cubic structure. From the patterns, the peak positions and half peak width of the (111) plane slightly change after doping, which implies that the structures have very small strain. The slight shift in the peak position which

is associated with the replacement of Ni^{2+} ions (0.69 Å) by Co^{2+} (0.745 Å), Cu^{2+} (0.73 Å), and Mn^{2+} (0.83 Å) ions of the larger radius is believed to be the cause of this situation. As a result of doping, the half peak widths clearly change with doping and the best crystallization was showed in the Co doped NiO films. There are no peaks related to other phases in XRD patterns which are probably related to low doping concentration (3 % at).

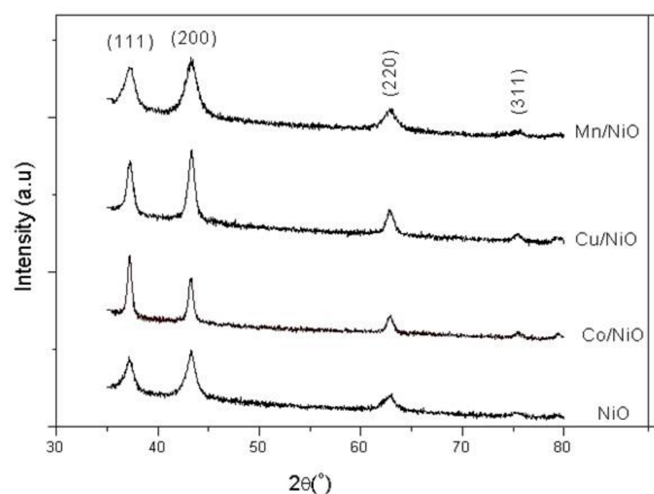

Figure 1. XRD patterns of un-doped and doped NiO films

The interplanar spacing dhkl values of un-doped and doped NiO films are calculated by using Bragg relation [25]:

$$2d_{hkl}\sin\theta = n\lambda \quad (3)$$

where n is the order of diffraction (usually n=1) and λ is the wavelength of X-ray radiation (1.5406 Å). The lattice parameters (a) of NiO cubic structure is calculated using the following relation [25]:

$$d = \frac{a}{\sqrt{h^2+k^2+l^2}} \quad (4)$$

Table 3 summarizes the positions of (111) peak, the calculated values of $d_{(111)}$, which shows deviations from the standard value of the lattice parameters a= 4.1770 Å taken from JCPDS card file data. This could be an indication of strain in the films and interpreted as the unit cell of the films undergoes contraction or expansion along a-axis. Table 3 summarizes the positions of (111) peak, the calculated values of $d_{(111)}$, which shows deviations from the standard value of the lattice parameters a= 4.1770 Å taken from JCPDS card file data. This could be an indication of strain in the films and interpreted as the unit cell of the films undergoes contraction or expansion along a-axis.

The average crystallite size of NiO was calculated from X-ray line broadening for (111) plane using the Scherer and the Williamson–Hall equation. Firstly, Scherer equation was used [25]:

$$D = \frac{0.9\lambda}{\beta cos\theta} \quad (5)$$

where β is the broadening of diffraction line measured at half of its maximum intensity (FWHM). Comparing the FWHM values corresponding to (111) plane, the broadening of the diffraction peak is observed for the films doped with Mn comparing to un-doped NiO film. The most probable explanation could be due to the increasing crystal defects. On the other hand, doping with Cu and Co has a positive effect on crystallinity. This can be attributed to the fact that at lower doping Co and Cu ions replace Ni ions substitutionally [26]. The average crystallite size of the samples was calculated to be in the range 11- 18 nm (Table 2). The texture coefficients (TC) have been calculated for well resolved (111), (220), and (200) crystallographic planes using the well-known equation below [27]:

$$TC = \frac{I_{(hkl)}/I_{0(hkl)}}{\frac{1}{N}\Sigma_N I_{(hkl)}/I_{0(hkl)}} \quad (6)$$

where $I_{(hkl)}$ is the measured intensity, $I_{0(hkl)}$ is the standard intensity, and N is the number of diffraction peaks. For a preferential orientation, the $TC_{(hkl)}$ values should be greater than one [13]. For all the films, the texture coefficient values are greater than one for the (111) plane. Calculated $TC_{(hkl)}$ values for different planes are listed in Table 4. The increase and decrease in the value of $TC_{(hkl)}$ are attributed to the reorientation effect of crystal in a given (hkl) direction due to the doping process (Fig. 2).

Table 3. (111) peak positions, interplanar spacing d, FWHM values and lattice parameter

Figure 2. Variation of texture coefficient of un-doped and doped NiO films

Films	2θ (deg)	*d*	FWHM	a_{111}
NiO	37.157	2.4177	0.664	4.1838
Cu-NiO	37.281	2.4099	0.609	4.1741
Co-NiO	37.259	2.4113	0.447	4.1765
Mn-NiO	37.281	2.4099	0.813	4.1792

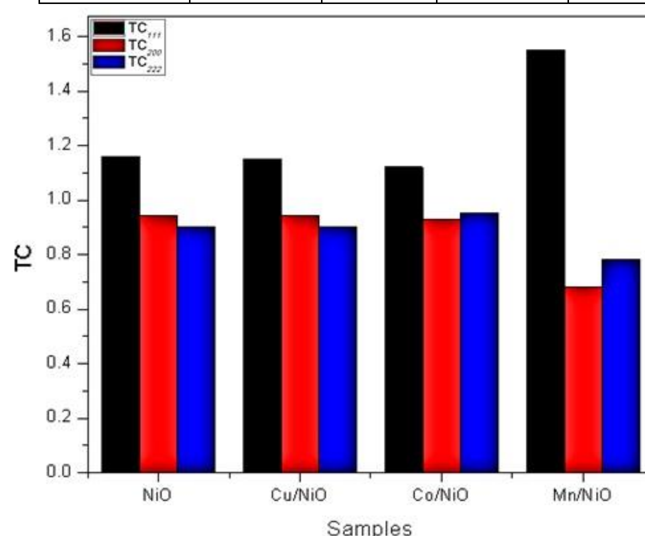

The lattice strain and crystallite size are two independent factors that contribute to the total peak broadening. The total

peak broadening is the sum of the contributions of crystallite size and strain present in the material. Secondly, the crystallite size and strain ε in the films have been determined from the XRD measurements by using the Williamson–Hall equation;

$$\frac{\beta cos\theta}{\lambda} = \frac{1}{D} + \varepsilon\frac{sin\theta}{\lambda} \quad (7)$$

where D is the average grain size, ε is the effective strain, β is the FWHM, θ is the Bragg diffraction angle, λ is the X-ray wavelength. [32]. The term (βcosθ) was plotted with respect to (4sinθ) for the preferred orientation (111), (200), and (220) peaks of NiO films as seen in Figure 3. Accordingly, the slope and y-intersect of the fitted line represent strain and particle size, respectively. The estimated strain and crystallite size values of the deposited films are listed in Table 4 and 5. The calculated grain sizes in both methods were matching with each other. The result is consistent with that of the XRD patterns.

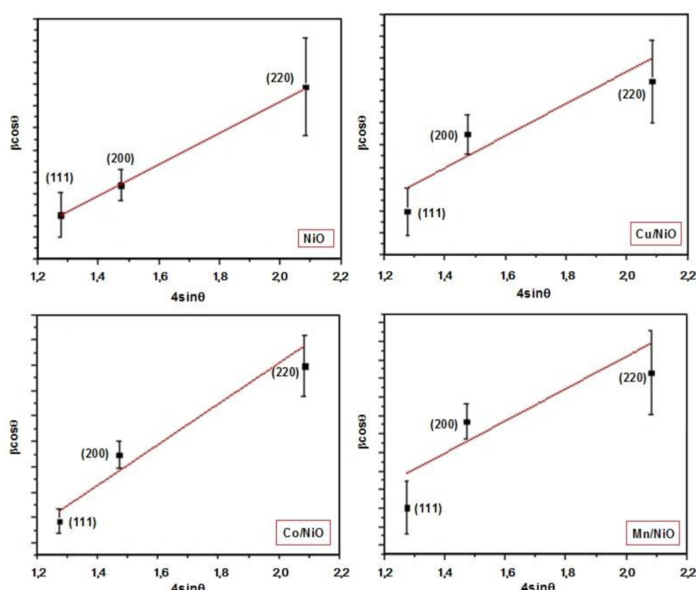

Figure 3. The W-H analysis of NiO films

Table 4. The *D* values, strain and *TC* of NiO films

Films	D (nm)		ε %
	Scherer	Williamson-Hall	
NiO	12	11.1± 1.4	0.25 ± 0.1
Cu-NiO	14	14± 1	0.13±0.04
Mn-NiO	11	7.8± 0.8	0.30 ± 0.1
Co-NiO	18	33.2± 6.2	0.28±0.05

Table 5. The TC values of NiO films

Films	TC (hkl)		
	(111)	(200)	(220)
NiO	1.16	0.94	0.90
Cu-NiO	1.15	0.94	0.90
Mn-NiO	1.12	0.93	0.95
Co-NiO	1.55	0.68	0.78

The relationship between grain size and diffraction angle for phase (111) is given in graph Fig. 4. As can be seen, the smallest grain size was obtained in cobalt doped nickel oxide film. This case can be supported XRD analysis (see Fig. 2). Co doped NiO films have the best crystalline level and the narrowest half peak width among doped NiO films. We think that crystallization increases due to the improvement of oxygen diffusion for Co doped NiO films. On the other hand, the increase in grain size decreased the grain boundaries and resulted in improvement of structural and optical properties. The similar results have been observed in other studies in the literature [40].

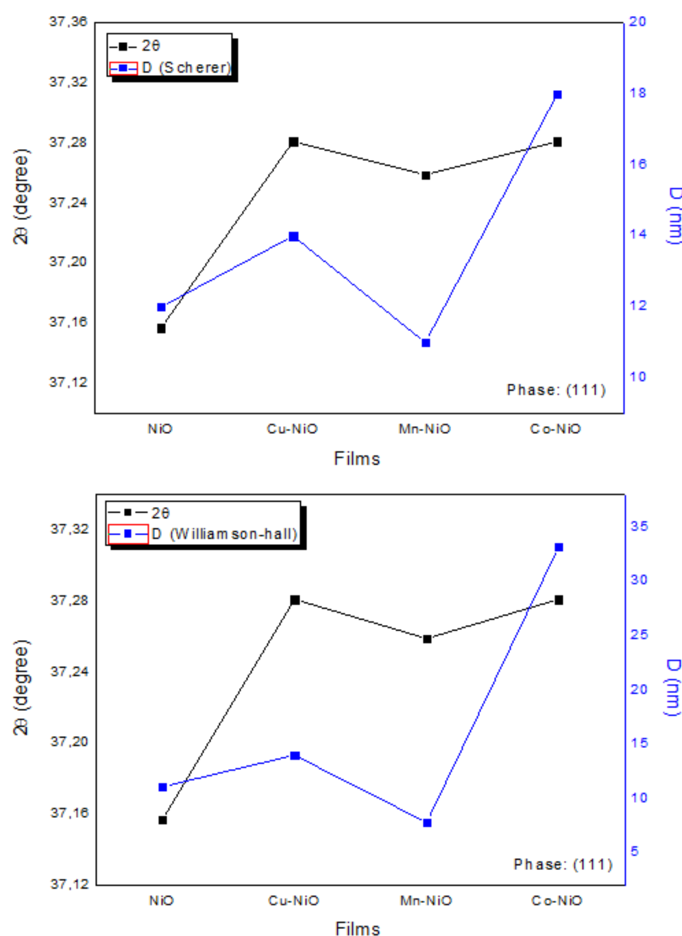

Figure 4. The variation of diffraction angle and crystallite size of undoped and doped NiO films for (111) phase

4.2. Optical characterization

The optical properties of NiO films were studied to investigate the effect of the doping on the optical transmittance, band gap, and Urbach energy. The absorbance spectra of the NiO films were taken in the wavelength range of 300-1100 nm at room temperature. Fig. 5 shows the optical absorbance spectra of NiO films doped with the Co, Cu, and Mn contents. It has been found that at the low wavelength region, the absorbance rises near the absorption edge at the UV region followed by a low absorbance with increasing the wavelengths. In this study, un-doped NiO film exhibited different absorbance edge structure comparing to doped NiO films, which were the best similar behavior Cu-doped films. Also, we can observe that absorbance edge of doped NiO films changed and become sharper with Co and Mn doping presenting the same absorbance edge.

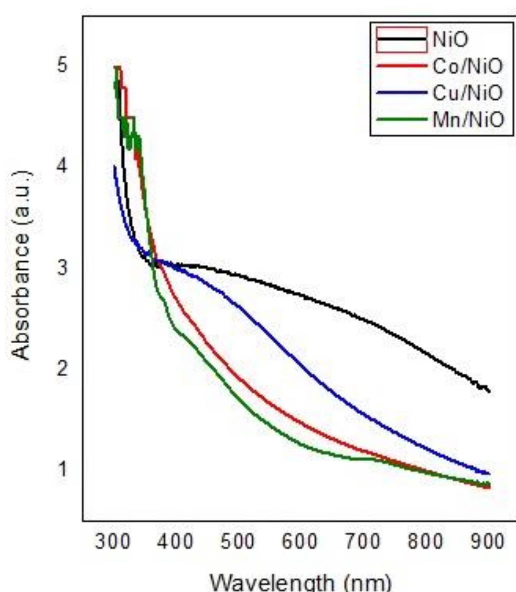

Figure 5. Absorbance spectra un-doped and doped NiO films

The optical band gap Eg is determined using the Tauc relation [28];

$$(\alpha h\nu)^{1/p} = A(h\nu - E_g) \quad (8)$$

where α is the absorption coefficient, E_g is the band gap corresponding to a particular transition occurring in the film, A is a constant, ν is the transition frequency and p can take the values 1/2, 3/2, 2 or 3, when the transitions are direct allowed, direct forbidden, indirect allowed and indirect forbidden respectively. The NiO is considered as a material with direct band gap energy and hence p=1/2 is expected for direct allowed transition. The band gap has been calculated by extrapolating the linear region of the plots $(\alpha h\nu)^2$ versus $h\nu$ on the energy axis (Figure 6). The values of the band gap were found to be ranging from 3.55 eV to 3.20 eV. These values are showed in Table 5 and clearly decrease with Cu/Mn/Co doping. As kwon, the energy band gap of NiO occurs between the O 2p states of the valence band and Ni 3d states of the conduction band. According to the optical measurements, the decrease in the optical band gap of doped NiO films with Cu/Mn/Co doping is due to the structural changes of NiO films. Since the XRD data show no clearly structural changes, local structural changes nearby the Cu/Mn/Co dopant elements may play a key role for the observed band gap narrowing. For Cu doped NiO films, the decrease in energy band gap from 3.55 to 3.28 eV may be due to increase in the width of donor levels of copper atoms and attributed to the increased in the grain size [41-43]. Similarly, the band gap values of Mn doped NiO films decrease because Mn ions may make holes and vacancies in the doped NiO lattice resulting in the reduction of the energy gap [44]. Similar results for band gap shrinkage were found by Baraman et al. for Mn doped NiO [45]. If we look closely, Co doped NiO films have the lowest band gap value. The reason for this decrease may be Co^{2+} oxidation state due to cobalt exists in Co^{2+} oxidation state in the sites occupied by cations in the host lattice. Also, Co ions and oxygen vacancies can constitute additional energy levels in the NiO band gap near the valence band edge. Consequently, both the increased sp-d exchange interactions between the band electrons and the localized d electrons of Co^{2+} cations and also the point defects deformation of band edges may be caused this decrease in E_g values. Similar results were found in the literature [46, 47].

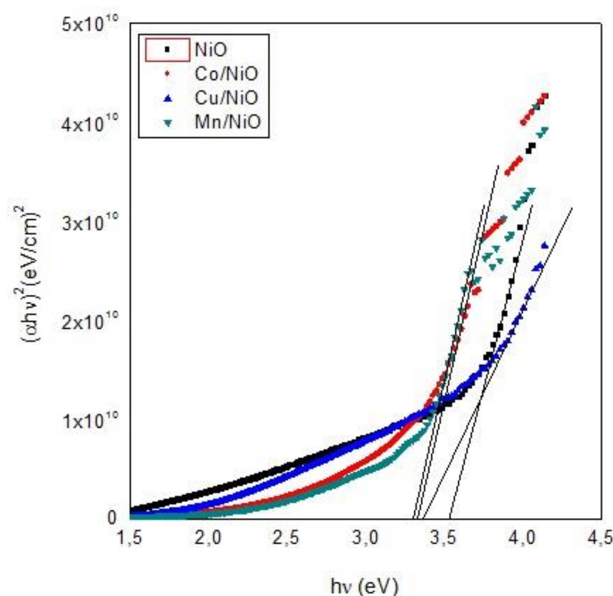

Figure 6. Optical band gap energy of un-doped and doped NiO films

As seen in Figure 7, the absorption coefficient dependence on photon energy in the spectral range of the near-band-edge empirically follows the exponential law (Urbach tail), which can be expressed as [29]:

$$\alpha(h\nu) = \alpha_0 \exp(h\nu/E_u) \quad (9)$$

where α_0 is a constant, E_u is Urbach energy which corresponds to the width of the band tail and could be determined as the width of the localized states. Usually, Eu depends on temperature and structural disorder describes the width of the localized states in the band gap region [30]. Fig. 7 shows the variation of $ln\alpha$ vs. photon energy for the films.

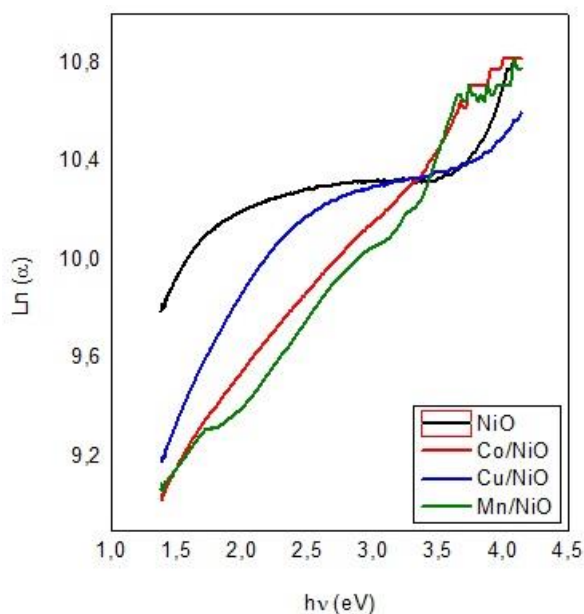

Figure 7. The Urbach plots of the undoped and doped NiO films

To obtain the width of Urbach tail, a linear fit was Herve - Vandamme, and Moss relations [31, 32, 35]. Both established in the linear portions of the curves and the results were listed in Table 6. E_u values change inversely with optical band gap. Also, the Urbach energy values give knowledge about local defects which create localized states in the band gap region [33]. The steepness parameter, $\sigma = kT/E_u$; characterizing the broadening of the optical absorption edge due to electron-phonon or exciton-phonon interactions [34] was also determined taking T =300 K and given in Table 5. The change in the band gap and Urbach energy of NiO films as a function of doping content is given in Fig. 8. The un-doped NiO films have higher band gap and Urbach energy values than Co, Cu, and Mn- doped NiO films.

Table 6. Some optical parameters of un-doped and doped NiO films

Films	E_g (eV)	E_u (meV)	$\sigma.10^{-2}$
NiO	3.55	344	7.47
Cu-NiO	3.28	317	8.11
Co-NiO	3.20	314	8.18
Mn-NiO	3.22	312	8.24

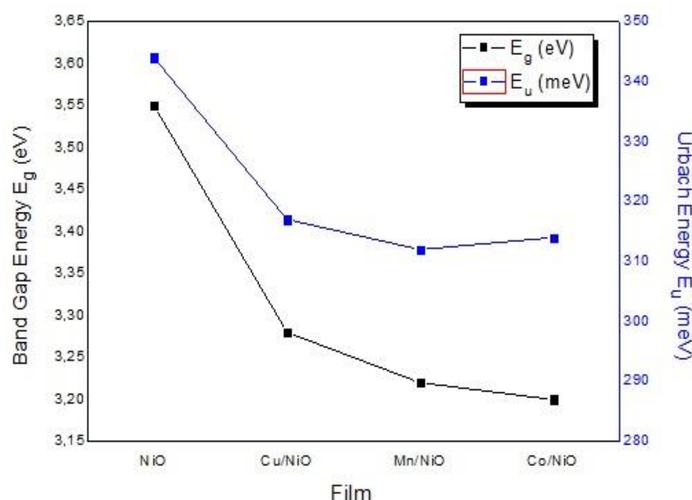

Figure 8. The change of the band gap and Urbach of the un-doped and doped NiO films

Refractive index (n) and the band gap energy (E_g) are the two important parameters that resolve the optical and electrical behavior of semiconductor thin films used for optoelectronic applications. Also, determination of the dielectric properties of films is especially important for diverse optoelectronic device applications. For this reason, we calculated the optical parameters such as refractive index, high-frequency and static dielectric constants for NiO films. There are many methods used to determine the optical parameters of thin films. We chose two different methods to determine refractive index and dielectric constants in our work. These methods are Herve – Vandamme and Moss relation. The common feature of these methods is that we can calculate the refractive index based on the band gap. The formulas used in the calculations are as follows:

Herve -Vandamme method

$$n = \sqrt{1 + \left(\frac{A}{E_g + B}\right)^2} \quad (10)$$

Moss relation is presented

$$n^4 = \frac{k}{E_g} \quad (11)$$

High-frequency dielectric constants

$$\varepsilon_0 = 18.52 - 3.08E_g \quad (12)$$

Static dielectric constants

$$\varepsilon_\infty = n^2 \quad (13)$$

where A and B are numerical constants with values of 13.6 and 3.4 eV, k is a constant with a value of 108 eV respectively [31, 32, 35, 36]. The change in the refractive index and dielectric constants of un-doped and doped NiO films as a function of doping content is given in Fig. 9. The calculated optical parameters (n, ε_∞ and ε_0) of the un-doped and doped

NiO films are listed in Table 7 and 8 for two models. It is clearly seen that the refractive index values increased upon doping with Co, Cu, and Mn elements with different rate of increase depending on the used models.

Table 7. The refractive index (*n*) of un-doped and doped NiO films

Films	Refractive Index (*n*)	
	Moss Relation	Herve-Vandamme
NiO	2.34	2.19
Cu-NiO	2.39	2.26
Co-NiO	2.41	2.29
Mn-NiO	2.40	2.28

Table 8. The dielectric constants of un-doped and doped NiO films

Films	Dielectric constants (ε_∞ and ε_0)			
	Moss Relation		Herve-Vandamme	
	ε_∞	ε_0	ε_∞	ε_0
NiO	5.51	7.58	4.82	7.58
Cu-NiO	5.73	8.41	5.14	8.41
Co-NiO	5.80	9.85	5.24	8.66
Mn-NiO	5.79	9.60	5.22	8.60

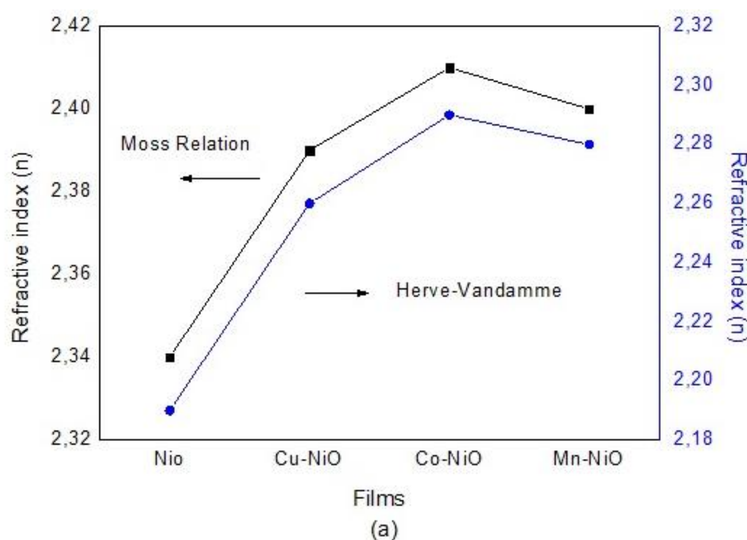

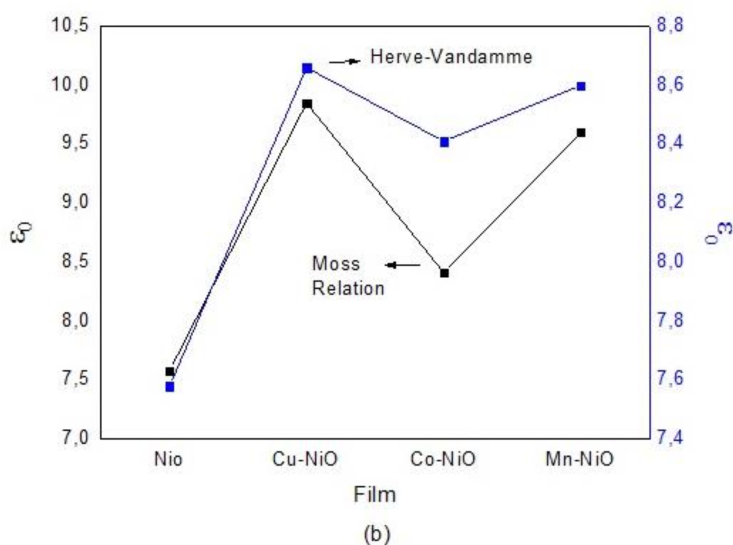

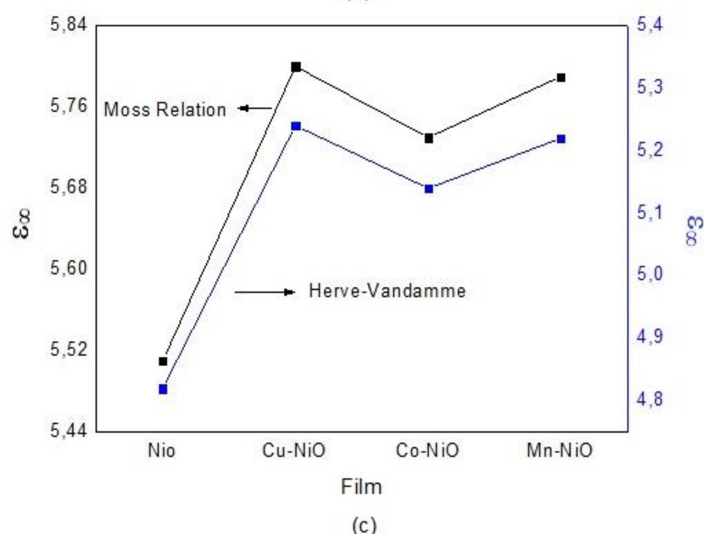

Figure 9. The change of the refractive index and dielectric constants of un-doped and doped NiO films.

4.3. Surface morphology

For the morphological investigation, a field emission scanning electron microscope (FESEM) was used. FESEM images were taken with In-Lens detector under 20 kV operating voltage. All films were coated with Au by means of an EMS sputter coater to dismiss the charging effect. SEM images are shown in Fig. 10 (a-d). From the micrographs, it is seen that the films consist of nanocrystalline grains with different size and clusters depending on the doping content. Fig. 10 (a) and 10 (d) correspond to un-doped and Mn-doped NiO films, respectively. Both films are similar in the microstructure, i.e., high degree of agglomeration in nanoparticles could be observed. Fig. 10 (b) corresponds to the Co-doped NiO film which exhibits the granular on the surface with different sizes were distributed throughout. The image in Fig. 10 (c) corresponds to Cu-doped NiO films

where "cauliflower" aggre gates are observed, which also contribute to light scattering.

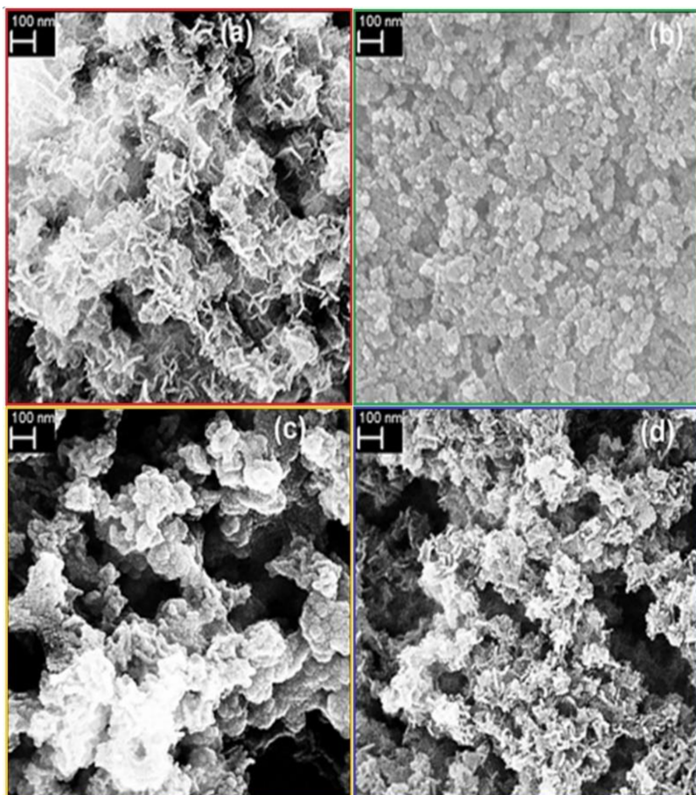

Figure 10. FESEM images of (a) un-doped, (b) Mn-doped, (c) Co-doped, and (d) Cu-doped NiO films

5. Conclusion

In this work, various transition metals (Cu, Co and Mn) were determined as dopant elements for NiO films and spray pyrolysis technique was used to deposition un-doped and doped NiO films on glass substrate. We present the effect of different transition metals on the structural, morphology and optical properties of the NiO films. We show that various transition metals (Cu, Co and Mn) were effectively added into the NiO films crystal lattice without significant structural change. The analysis of XRD patterns revealed that all films have face-centered cubic phase. The average crystallite size, lattice parameter, micro-strain and texture coefficient value changes with doping, resulting in the structural variation. Un-doped and doped NiO films showed (111) preferential growth plane orientation. The texture coefficient TC(111) was not change but the half peak width clearly change with doping. As a result of doping, the best crystallization was showed in the Co doped NiO films. The grain size was calculated two different methods (Scherer and Williamson-Hall) and the results of these methods were coherent with each other. The optical measurements indicate that the band gap values decreased with doping and Co doped NiO films exhibited a minimum band gap of 3.20 eV. The refractive index and dielectric constant values of NiO films were calculated using Moss relation and Herve-Vandamme formula and these values increased with doping. The obtained results lead us to resolve that the crystalline structure, optical parameters and morphology of the NiO films can be easily tailored with doping transition metals using a cost-effective spray pyrolysis technique.

Acknowledgement:
Authors are thankful to Prof. Dr. Evren TURAN and her doctoral students, Eskişehir Technical University, Eskişehir, Turkey, for providing some processing and the facilities of XRD and FESEM analysis.

References

[1] M. Guziewicz, J. Grochowski, M. Borysiewicz, E. Kaminska, J. Z. Domagala, W. Rzodkiewicz, B. S. Witkowski, K. Golaszewska, R. Kruszka, M. Ekielski, A. Piotrowska, Optica Applicata XLI 2 (2011) 431
[2] A. Kalam, A. S. Al-Shihri, A. G. Al-Sehemi, N.S. Awwad, G. Du, T. Ahmad, Superlattices and Microstructures 55 (2013) 83
[3] J. G. Cook, F. P. Koffyberg, Solar Energy Materials 10(1) (1984) 55
[4] C. G. Granqvist, Solar Energy Mater. and Solar Cells 92 (2008) 203
[5] P. C. Chou, H. I. Chen, I. P. Liu, C. C. Chen, J. K. Liou, International Journal of Hydrogen Energy 40(1) (2015) 729
[6] J. L. Yin, J. Y., International Journal of Hydrogen Energy 39 (2014)16562
[7] I. Hotový, J. Huran, J. Janík, A. P. Kobzev, Vacuum 51(2) (1998) 157
[8] W. Shın, N. Murayama, Materials Letters 45(6) (2000) 302
[9] A. Azens, L. Kullman, G. Vaıvars, H. Nordborg, C.G. Granqvıst, Solid State Ionics 113–115 (1998) 449
[10] L. M. Choı, S. Im, Applied Surface Science 244 (1–4) (2005) 435
[11] I. Hotový, J. Huran, L. Spıess, R. Čapkovıc, Š. Haščík, Vacuum 58 (2–3) (2000) 300
[12] H. L. Chen, Y. M L.u, W. S. Hwang, Surface and Coatings Technology 198 (2005)138
[13] I. Y. Syukri, T. Ban, Y. Ohya, Y. Takahashi, Thin Solid Films 422 (2002) 48
[14] J. Yu, D. Kim, Powder Technology 235 (2013)1030
[15] M. A. Ben, A. Boukhachem, K. Boubaker, M. Amlouk, Materials Science in Semiconductor Processing 27 (2014) 994
[16] Y. A. K. Reddy, A. S. Reddy, P. S.Reddy, Journal of Material Science Technology 29 (7) (2013) 647
[17] L. Lei, K.S. Hui, K. N. Hui, H. W. Park, D. H. Hwang, S. Cho, S. K. Lee, P. K. Song, Y. R. Cho, H. Lee, Y.G. So, W. Zhou, Materials Letters 68 (2012) 283
[18] T. M. Roffi, S. Nozaki, K. Uchida, Journal of Crystal Growth 451 (2016) 57
[19] M. Ristova, J. Velevska, M. Ristov, Solar Energy Materials Solar Cells 71 (2002) 219
[20] J. D. Desai, S. K. Min, K. D. Jung, O. S. Joo, Applied Surface Science 253 (2006) 1781 [21] P. Mohanty, R. Chandana, P. Mallick, R. Biswal, N.C. Mishra, Physica B. 405 (2010) 2711

[22] Z. T. Khodair, A. A. Kamil, Y. K. Abdalaah, Physica B: Condensed Matter. 503 (2016) 55 [23] Z. Halem, N. Halem, M. Abrudeanu, S. Chekroude, C. Petot, G. Petot-Ervas, Solid State Ionics 297 (2016) 13
[24] Y. Li, X. H. Li, Z. X. Wang, H. J. Guo, T. Li, Ceramics International 42 (2016) 14565
[25] B. D. Cullity, S. R. Stock, Elements of X-ray Diffraction, Prentice-Hall, New Jersey, 2001
[26] R. Sharma, A. D. Acharya, S. Moghe, S. B. Shrivastava, M. Gangrade, Materials Science in Semiconductor Processing 23 (2014) 42
[27] H.H. Huang, M.H. Hon, Journal of Crystalline Growth 222 (2001) 540
[28] J. I. Pankove, Optical Processes in Semiconductors; Dover Publication: Mineola, New York,1975
[29] F. Urbach, Physical Review 92 (1953) 1324
[30] K. Boubaker, European Physical Journal B. 84 (2011) 235
[31] F. Mezrag, W. M. Kara, N. Bouarissa, Physica B: Condensed Matter. 405 (2010) 2272
[32] G. Williamson, W. Hall, Acta Metall. 1 (1953) 22
[33] M. Fterich, F. B. Nasr, R. Lefi, M. Toumi, S. Guermazi, Materials Science in Semiconductor Processing 43, (2016) 114
[34] H. Mahr, Physics Review 125, (1962) 1510
[35] P. Herve, L. K. J. Vadamme, Infraed Physics and Technology 35 (1994) 609
[39] M. Mekhnache, A. Drici, L. Saad Hamideche, H. Benzarouk, A. Amara, L. Cattin, J.C. Bernede, M. Guerioune, Superlattices Microstruct 49 (2011) 510
[40] Abdallah Diha, Said Benramache, Boubaker Benhaou, Optik-International Journal for Light and electron optics 172 (2018) 832
[41] Manouchehri, D. Mehrparvara, R. Moradiana, K.Gholami, T.Osati, Optik 27 (2016) 8124
[42] Rufus O. Ijeh, Assumpta C. Nwanya, Agnes C. Nkele, Itani G. Madiba, Z. Khumalo, A.K.H. Bashir, R.U. Osuji, M. Maaza, Fabian I. Ezema, Physica E: Low-dimensional Systems and Nanostructures 113 (2019) 233
[43] Moghe, A.D. Acharya, R. Panda, S.B. Shrivastava, M. Gangrade, T. Shripathi,V. Ganesan, Renew. Energy 46 (2012) 43
[44] M. Baraman, S. Paul, A. Sarkar, AIP Conf. Proc 1536 (2013) 427
[45] J. Al Boukharia,⁎ , L. Zeidana , A. Khalafb , R. Awad, Chemical Physics 516 (2019) 116
[46] P.A. Sheena, H. Hitha, A. Sreedevi , Thomas Varghese, Material Chemistry and Physics 229 (2019) 412
[47] R. He, R.K. Hocking, T. Tsuzuki, Mater. Chem. Phys. 132 (2012) 1035–1040